Opto-Electronic Advances

Supplementary information

2020, Vol. 3, No. 12

DOI: 10.29026/oea.2020.200028

Athermal third harmonic generation in micro-ring resonators

Shao Hao Wang[1,6]*, Yuhua Li[2,7], Brent E. Little[3], Leiran Wang[3,4], Xiang Wang[5], Roy R. Davidson[5] and Sai Tak Chu[2]*

[1]FZU-Jinjiang Joint Institute of Microelectronics, Jinjiang Science and Education Park, Fuzhou University, Jinjiang 362200, China. [2]Department of Physics, City University of Hong Kong, Kowloon Tong, Hong Kong 999077, China. [3]State Key Laboratory of Transient Optics and Photonics, Xi'an Institute of Optics and Precision Mechanics, Chinese Academy of Sciences, Xi'an 710119, China. [4]University of Chinese Academy of Sciences, Beijing 100049, China.[5]QXP Technology, Xi'an 710311, China. [6]Department of Microelectronics Science and Technology, Qi Shan Campus, Fuzhou University, Fuzhou 350108, China. [7]Key Laboratory of Optical Field Manipulation of Zhejiang Province, Department of Physics, Zhejiang Sci-Tech University, Hangzhou, Zhejiang 310018, China

*Correspondence: S H Wang, E-mail: shwang@fzu.edu.cn; S T Chu, E-mail: saitchu@cityu.edu.hk

This file includes:

Supplementary information for this paper is available at https://doi.org/10.29026/oea.2020.200028

Section 1: Thermal dynamics model

In micro-ring resonators (MRRs), the dependency of the N-th resonance wavelength λ_r on the chip temperature T obeys[S1]

$$N = \frac{2\pi R}{\lambda_r}(1 + \varepsilon\delta T)\left(n_0 + \frac{\mathrm{d}n}{\mathrm{d}T}\delta T\right), \tag{S1.1}$$

where, $\delta T = T - T_0$ is the difference between T and the "cold-cavity" chip temperature T_0 which gives rise the waveguide refractive index n_0. Here, ε is the expansion coefficient and R is the radius of the MRR. The resonance wavelength λ_r thus becomes a function of δT

$$\lambda_{ir}(\delta T) \cong \lambda_{i0}\left[1 + \left(\varepsilon + \frac{1}{n_{i0}}\frac{\mathrm{d}n}{\mathrm{d}T}\right)\delta T_i\right] \equiv \lambda_{i0}(1 + \xi_i T_i), \quad (i = \mathrm{p}, \mathrm{t}) \tag{S1.2}$$

where, λ_{i0} and ξ_i, i = p, t, are the cold-cavity resonance wavelengths and the corresponding linear thermo-optics (TO) coefficients of the pump and the TH modes.

In silicon-rich complementary metal-oxide-semiconductor (CMOS) compatible platforms, the nonlinear TO behavior invoked by the intra-cavity optical power depends on the temperature difference ΔT between the mode volume (local heat) and the chip (at T) [S1]. The rate equation of the absorbed heat q_{gen} is proportional to the intra-cavity pump power P_{p} which gives

$$\frac{\mathrm{d}q_{\mathrm{gen}}}{\mathrm{d}t} = P_{\mathrm{p}}\frac{Q_{\mathrm{p}}}{Q_{\mathrm{aa}}}, \tag{S1.3}$$

where, Q_{p} and Q_{pa} are the loaded Q of pump and Q-factor relating to the pump absorption, respectively. For the corresponding net heat diffusion is taken as

$$\frac{\mathrm{d}q_{\mathrm{dif}}}{\mathrm{d}t} = U\Delta T(t), \tag{S1.4}$$

where, $U = KL_{\mathrm{eff}}/S_{\mathrm{eff}}$ is the effective thermal conductivity between the cavity mode volume and the chip, in J/(s·°C). Here, K is material thermal conductivity in W/(m·K) and S_{eff} is the area of effective surface of the intra-cavity pump mode and L_{eff} is the effective length from the cavity mode volume to the chip. The rate equation of the accumulated net heat ΔT in the cavity mode volume thus becomes

$$\frac{\mathrm{d}\Delta T}{\mathrm{d}t} = \frac{1}{C_p}\left(\frac{\mathrm{d}q_{\mathrm{gen}}}{\mathrm{d}t} - \frac{\mathrm{d}q_{\mathrm{dif}}}{\mathrm{d}t}\right) = \frac{Q_{\mathrm{p}}}{C_p Q_{\mathrm{pa}}}P_{\mathrm{p}} - \frac{U}{C_p}\Delta T(t), \tag{S1.5}$$

where, C_p is the heat capacity in J/°C.

Section 2: Thermal dynamics THG model with nonlinear TO and Kerr effects

For the pump and third harmonics (TH) emission, if we assume they have nearly the same group velocities by neglecting their counter propagation modes then the spatiotemporal slowly varying envelope of their optical fields will be consistent with the choice of the moving reference frame. We can further neglect the high-order dispersion terms if the discussion is only restricted to those that are nearly phase matched and have narrow linewidths. According to the thermal dynamics model described in Section 1, we can write a set of time-domain rate equations describing the dynamics of third harmonics generation (THG) in MRRs as[S2-S5],

$$\frac{\mathrm{d}a_\mathrm{p}}{\mathrm{d}t}=\left[-i\Omega_\mathrm{p}'-\frac{\kappa_p}{2}\right]a_\mathrm{p}-i\hbar\omega_\mathrm{p}\left(g_\mathrm{pp}\left|a_\mathrm{p}\right|^2+g_\mathrm{pt}|a_\mathrm{t}|^2\right)a_\mathrm{p}-3ig_\mathrm{TH}\hbar\omega_\mathrm{p}a_\mathrm{p}^*a_\mathrm{p}^*a_\mathrm{t}-i\sqrt{\kappa_\mathrm{ae}}p_i\,, \tag{S2.1}$$

$$\frac{\mathrm{d}a_\mathrm{t}}{\mathrm{d}t}=\left[-i\Omega_\mathrm{t}'-\frac{\kappa_\mathrm{t}}{2}\right]a_\mathrm{t}-i\hbar\omega_\mathrm{p}\left(g_\mathrm{tt}|a_t|^2+g_\mathrm{tp}\left|a_\mathrm{p}\right|^2\right)a_\mathrm{t}-ig_\mathrm{TH}\hbar\omega_\mathrm{p}a_\mathrm{p}^3\,, \tag{S2.2}$$

$$\frac{\mathrm{d}\Delta T}{\mathrm{d}t}=\frac{Q_\mathrm{p}}{C_pQ_\mathrm{pa}}\frac{v_\mathrm{gp}}{2\pi R}\left|a_\mathrm{p}\right|^2\hbar\omega_\mathrm{p}-\frac{U}{C_p}\Delta T(t)\,. \tag{S2.3}$$

where, $\left|a_\mathrm{p}\right|^2=I_\mathrm{p}/\hbar\omega_\mathrm{p}$ and $|a_\mathrm{t}|^2=I_\mathrm{t}/3\hbar\omega_\mathrm{p}$ are the photon numbers of intra-cavity pump and TH emission. Here, ω_p is angular frequency of extremal pump laser and I_p and I_t are the intra-cavity energy of the pump and TH emission. $\Omega_\mathrm{t}'(\delta T)=3\omega_\mathrm{p}-\omega_\mathrm{tr}(\delta T)$ and $\Omega_\mathrm{p}'(\delta T)=\omega_\mathrm{p}-\omega_\mathrm{pr}(\delta T)$ are the frequency detuning from the resonance peak of the TH emission and corresponding pump wavelength. ω_{i0} and ω_{ir}, i = p, t, are the cold-cavity resonance frequencies and resonance frequencies at δT of the pump and TH emission, respectively. κ_p, κ_t, and κ_pe are the overall loss of the pump, the overall loss of TH wave and the externally coupling rate of pump. On the right-hand side of Eqs. (S2.1) and (S2.2), the third term is the self-phase modulation (SPM), the fourth term is the cross-phase modulation (XPM), and the fifth term is TH coupling effects. Here, g_pp and g_tt are the nonlinear parameters, and g_pt and g_tp are the XPM coefficients of the pump and TH emission, while g_TH is the growth rate of the THG. In Eq. (S2.1), the last term refers to coupled input pump power. If we define $|p_x|^2=P_x/\hbar\omega_\mathrm{p}$, x = in, through, drop, are the amplitudes of the input pump, the through port pump, and the drop port pump, the dependences of p_through and p_drop to a_p can be written as

$$p_\mathrm{through}=p_\mathrm{in}-i\sqrt{\kappa_\mathrm{pe}}a_\mathrm{p}\,, \tag{S2.4}$$

$$p_\mathrm{drop}=-i\sqrt{\kappa_\mathrm{pe}}a_\mathrm{p}\,. \tag{S2.5}$$

If we consider the intra-cavity pump power induced ΔT, we can rewrite Eqs. (S1.2) as

$$\lambda_{ir}(\delta T,\Delta T)\equiv 2\pi c/\omega_{ir}\cong\lambda_{i0}[1+\xi_i\delta T+\xi_i'\Delta T]\,,\quad (i=p,t) \tag{S2.6}$$

where, ξ_p' and ξ_t' are the nonlinear TO factors of the pump and TH modes. At $\delta T=0$, the cold cavity detunings become $\Omega_\mathrm{p}=\Omega_\mathrm{p}'(0)=\omega_\mathrm{p}-\omega_\mathrm{p0}$ and $\Omega_\mathrm{t}=\Omega_\mathrm{t}'(0)=3\omega_\mathrm{p}-\omega_\mathrm{t0}$. For silicon rich CMOS compatible waveguides, since $\xi_\mathrm{b}\delta T+\xi_\mathrm{b}'\Delta T\ll 1$, Eq. (S2.6) yields

$$\Omega_i^{'}=\Omega_i+\frac{\xi_i\delta T+\xi_i^{'}\Delta T}{1+\xi_i\delta T+\xi_i^{'}\Delta T}\omega_{i0}\cong\Omega_i+\left(\xi_i\delta T+\xi_i^{'}\Delta T\right)\omega_{i0}\,.\quad (i=p,t) \tag{S2.7}$$

For typical THG in MRRs, since the intra-cavity power of the pump is much larger than that of the TH wave, we can neglect all of the SPM terms, XPM term and pump depletion induced by TH wave. By replacing Ω_p' and Ω_t' using Eqs. (S2.7), we can rewrite Eqs. (S2.1)-(S2.2) in the nondepletion form of

$$\frac{\mathrm{d}a_\mathrm{p}}{\mathrm{d}t}=\left[-i\Omega_\mathrm{p}-i(\xi_\mathrm{p}\delta T+\xi_\mathrm{p}'\Delta T)\omega_\mathrm{p0}-\frac{\kappa_\mathrm{p}}{2}\right]a_\mathrm{p}-ig_\mathrm{pp}\hbar\omega_\mathrm{p}\left|a_\mathrm{p}\right|^2a_\mathrm{p}-i\sqrt{\kappa_\mathrm{ae}}p_i\,, \tag{S2.8}$$

$$\frac{\mathrm{d}a_\mathrm{t}}{\mathrm{d}t}=\left[-i\Omega_\mathrm{t}-i(\xi_\mathrm{t}\delta T+\xi_\mathrm{t}'\Delta T)\omega_\mathrm{t0}-\frac{\kappa_\mathrm{t}}{2}\right]a_\mathrm{t}-ig_\mathrm{tp}\hbar\omega_\mathrm{p}\left|a_\mathrm{p}\right|^2a_t-ig_\mathrm{TH}\hbar\omega_\mathrm{p}a_\mathrm{p}^3\,. \tag{S2.9}$$

Section 3: Thermal self-stability of THG in microcavities

In Section 2, Eqs. (S2.8)-(S2.9) describe the dynamics of the pump and the TH emission on a reference frame moving at the group velocity v_{gp}[S6]. Even using continuous-wave (CW) external pump, steady nonuniform intra-cavity energy distribution still exists, such as Turing rolls or soliton[S7]. However, the intra-cavity energy induced mode volume heat does not follow this moving frame. Thus, for pump and TH wave, the phase of intra-cavity spatiotemporal pulse is affected by both intraframe Kerr effect and the out-of-frame averaged thermal effects.

In this work, our discussion requires steady and uniform intra-cavity power distribution for both pump and TH waves. In this case, both optical power and net mode volume heat are evenly distributed on the ring cavity, in which thermal effects with Kerr effect are aligned regardless the reference frame. This uniform intra-cavity power distribution can be experimentally achieved by choosing resonance modes with large normal dispersion. If we input a CW external pump to these modes and sweep the pump wavelength at a low speed, a thermally self-stabilized system will be built up to maintain the equilibrium between the intra-cavity power induced absorbed-heat and the dissipated-heat, which can be appreciated by calculating $\partial\Delta T/\partial t = 0$, finding the steady-state solution of Eq. (S2.3),

$$\frac{Q_{\mathrm{p}}}{Q_{\mathrm{pa}}}\frac{v_{\mathrm{gp}}I_{\mathrm{p}}}{2\pi R} = U\Delta T\,. \tag{S3.1}$$

By using the same steady-state assumption and substituting Eq. (S3.1) in Eq. (S2.8), we have

$$\left[-i\Omega_{\mathrm{p}} - i\xi_{\mathrm{p}}\omega_{\mathrm{p0}}\delta T - \frac{\kappa_{ip}}{2}\right]a_{\mathrm{p}} - i\left(\Theta_{\mathrm{p}} + g_{\mathrm{pp}}\right)I_{\mathrm{p}}a_{\mathrm{p}} - i\sqrt{\kappa_{\mathrm{pe}}}p_i = 0\,, \tag{S3.2}$$

where, we define $\Theta_{\mathrm{p}} = \frac{Q_{\mathrm{p}}\xi_{\mathrm{p}}'\omega_{p0}}{UQ_{pa}}\frac{v_{gp}}{2\pi R}$ as the thermal nonlinear coefficient of the pump in rad/J. From Eq. (S3.2), the dependence of pump cold resonance detuning Ω_{p} to the chip temperature and the intra-cavity pump energy of the MRR can be written as[S8]

$$\Omega_{\mathrm{p}} = -\xi_{\mathrm{p}}\omega_{\mathrm{p0}}\delta T - \left(\Theta_{\mathrm{p}} + g_{\mathrm{pp}}\right)I_{\mathrm{p}} \pm \sqrt{\kappa_{\mathrm{pe}}\frac{P_i}{I_{\mathrm{p}}} - \frac{\kappa_{\mathrm{p}}^2}{4}}\,. \tag{S3.3}$$

Note that in Eq. (S3.3), $\Theta_{\mathrm{p}} >> g_{\mathrm{pp}}$ in highly doped silica glass and the SPM terms can be neglected.

Figure S1(a) plots Ω_{p} as a function of I_{p} at different T using Eq. (S3.3). The parameters used for plotting are shown in Table S1. As shown in Fig. S1(a), when up sweeping the wavelength of CW input pump at a fixed power, the intra-cavity pump energy increases due to the reduction of effective pump detuning Ω_{p}' which heats up the pump mode volume of MRR and leads to redshift of the resonance frequency of the pump mode. Once the sweep speed of the pump wavelength is slow enough so that the cavity can be thermally self-stabilized, it produces a triangular shape response over a board spectrum range[S2-S3]. Figure S1(a) shows that Eq. (S3.3) can well describe the chip temperature change δT induced pump resonance drifting.

For TH wave, by using the same steady-state assumption and substituting Eq. (S3.2) in Eq. (S2.9), we have

$$\left(-i\Omega_{\mathrm{t}} - i\xi_{\mathrm{t}}\delta T\omega_{\mathrm{t0}} - \frac{\kappa_t}{2}\right)a_{\mathrm{t}} - i\left(\Theta_{\mathrm{t}} + g_{\mathrm{tp}}\right)I_{\mathrm{p}}a_t = ig_{\mathrm{TH}}\hbar\omega_{\mathrm{p}}a_{\mathrm{p}}^3\,, \tag{S3.4}$$

where, $\Theta_{\mathrm{t}} = \xi_{\mathrm{t}}'\omega_{\mathrm{t0}}/\tau_{\mathrm{p}}$ is the nonlinear TO coefficient of the TH emission. In Eq. (S3.4), the term of $\Omega_{\mathrm{NL}} = (\Theta_t + g_{\mathrm{tp}})I_{\mathrm{p}}$ is the overall nonlinear phase mismatch in THG. From Eq. (S3.4), we can analytically express the dependence of TH power as

$$I_{\mathrm{t}} = \frac{12g_{\mathrm{TH}}^2I_{\mathrm{p}}^3}{\kappa_{\mathrm{t}}^2 + 4\left[\Omega_{\mathrm{t}} + \xi_{\mathrm{t}}\omega_{\mathrm{t0}}\delta T + \left(\Theta_{\mathrm{t}} + g_{\mathrm{tp}}\right)I_{\mathrm{p}}\right]^2}\,. \tag{S3.5}$$

In Eq. (S3.5), we notice that THG energy is not only determined by the product of g_{TH} and I_{p}, it also depends on the loss of the TH mode κ_{t}, as well as the linear and nonlinear TO phase mismatch. In Eq. (S3.5), the term of $\xi_{\mathrm{t}}\omega_{\mathrm{t0}}\delta T$ corresponds to chip temperature δT induced linear TO phase mismatch and the terms of $\Theta_{\mathrm{t}}I_{\mathrm{p}}$ and $g_{\mathrm{tp}}I_{\mathrm{p}}$ denote nonlinear TO effect and Kerr effect induced phase mismatch, respectively, both of which are proportional to I_{p}.

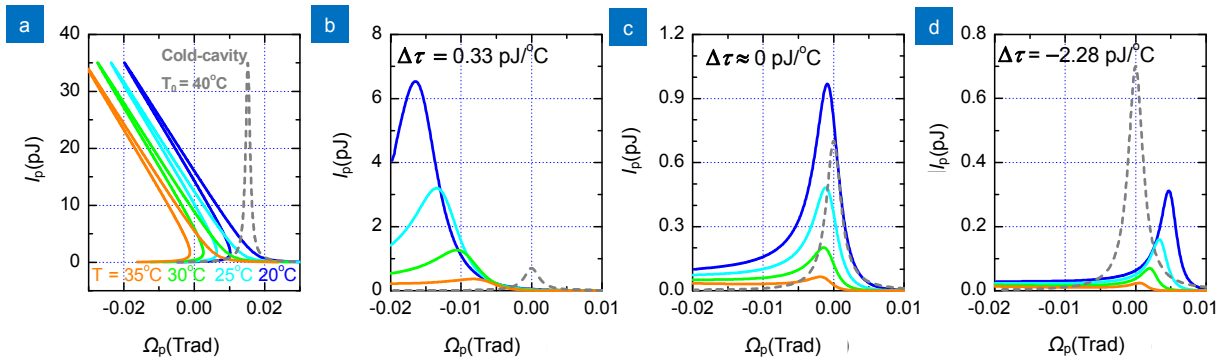

Fig. S1 | Prediction of generating TH modes with configurable TDWS when with different thermal mismatch $\Delta\tau$. (**a**) pump resonance shift plotting as a function of intra-cavity pump energy I_p by using Eq. (S3.2) when T = 20°C (blue lines), 25°C (light blue lines), 30°C (light green lines), and 35°C (orange lines). (**b – d**) used the same line styles for different T as in (a). The cold cavity pump resonance linewidth at T_0 = 40°C is also shown in gray dashed line. Corresponding spectra of TH resonance plotting as a function of Ω_p when $\Delta\tau > 0$ (b), $\Delta\tau \approx 0$ (c), $\Delta\tau < 0$ (d), under different T using Eq. (S3.5). In (b – d), the parameters are the same expects for $\Theta_t = 7 \times 10^8$ rad/pJ in (b) for $\Theta_t = 4 \times 10^8$ rad/pJ in (c), and for $\Theta_t = 10^8$ rad/pJ in (d). In (b – d), the cold cavity TH resonance neglecting the overall nonlinear phase mismatch Ω_{NL} is also shown in gray dashed line by assuming I_p = 15 pJ.

Table S1 | List of parameters used in Fig. S1.

Parameter	Description	Value	Units
T_0	The cold cavity chip temperature	40	°C
λ_{p0}	The pump resonance wavelength at T_0	1550	nm
ξ_p	The linear TO coefficient of the pump mode	10^{-6}	1/°C
ξ_t	The linear TO coefficient of the TH mode	4×10^{-7}	1/°C
Θ_p	The nonlinear TO redshift rate of the pump mode	10^9	rad/pJ
κ_{pe}	The externally coupling rate of the pump mode	2×10^8	s^{-2}
P_i	The input pump power	0.1	W
g_{TH}	The growth rate of THG	10^6	pJ^{-2}
Q_p	Q-factor of the pump mode	5×10^5	
Q_{TH}	Q-factor of the TH mode	3×10^5	

It is plotted in Figs. S1(b)–S1(d) the corresponding spectra of TH resonance as a function of Ω_p using Eq. (S3.5). The triangular pump response as shown in Fig. S1(a) tilts the shape of TH resonance response. In this case, the overall nonlinear phase mismatch redshifts the resonance of TH mode and broadens the linewidth of TH resonance ($\Delta\omega_t' > \Delta\omega_t$). Once thermal matched, i.e. $\Delta\tau \approx 0$, chip temperature independent THG can be achieved as shown in Fig. 1(c), which is known as athermal modes. When the thermal mismatch $\Delta\tau > 0$, since the linear TO phase mismatch over-compensates the nonlinear TO phase mismatch, the resonance of TH mode blueshifts when δT decreases as shown in Fig. S1(b). Fig. S1(d) shows the case of under linear TO compensation when $\Delta\tau < 0$ in which the resonance of TH mode redshifts when δT decreases.

The results of Figs. S1(b)–S1(d) indicate that Eq. (S3.5) can well describe the dependence of TH resonance on δT. With this model we are able to predict the visible THG pumped with the telecom wavelengths with positive, negative or even zero temperature dependent wavelength shift (TDWS).

Section 4: Linear and nonlinear TO phase mismatches in THG

From the model of Eq. (S3.4), we can determine the overall THG phase mismatch, which consists of the thermal phase mismatch and Kerr nonlinear mismatch Ω_{KNL}, by using Eq. (S2.7). The propagation constants of the pump and TH waves can thus be written as

$$\beta_{\mathrm{p}}(\delta T,\Delta T)=\frac{n_{0\mathrm{p}}\omega_{\mathrm{pr}}}{3c}+\Omega_{\mathrm{t}}'\frac{n_{\mathrm{gp}}}{3c}+\Omega_{\mathrm{t}}'^{2}\frac{\beta_{2,\mathrm{pr}}}{18}+\cdots, \tag{S4.1}$$

$$\beta_{\mathrm{t}}(\delta T,\Delta T)=\frac{n_{0\mathrm{t}}\omega_{\mathrm{tr}}}{c}+\Omega_{\mathrm{t}}'\frac{n_{gt}}{c}+\Omega_{\mathrm{t}}'^{2}\frac{\beta_{2,\mathrm{tr}}}{2}+\cdots, \tag{S4.2}$$

where, n_{0i} and $n_{\mathrm{g}i}$, $i = p, t$, are the effective refractive indices and group indices of the pump and TH waves, respectively. Here, c is the speed of light in vacuum and $\beta_{2,ir}$, i = p, t, are the group velocity dispersion (GVD) parameter at the resonances of the pump and TH waves, respectively[S9]. From Eq. (S4.1) and Eq. (S4.2), we get the expression of $\Delta\beta_{\mathrm{T}}$

$$\Delta\beta_{\mathrm{T}}(\delta T,\Delta T)=3\beta_{\mathrm{p}}-\beta_{\mathrm{t}}\approx\frac{\Delta n_0\omega_{br}}{c}+\frac{\Delta n_{\mathrm{g}}\Omega_{\mathrm{t}}'}{c}+\frac{\Omega_{\mathrm{t}}'^{2}}{6}\left(\beta_{2,\mathrm{pr}}-3\beta_{2,\mathrm{tr}}\right), \tag{S4.3}$$

where, $\Delta n = n_{0\mathrm{p}} - n_{0\mathrm{t}}$ and $\Delta n_{\mathrm{g}}=n_{\mathrm{gp}}-n_{\mathrm{gt}}=\frac{c}{R}\left(\frac{1}{FSR_{\mathrm{p}}}-\frac{1}{FSR_{\mathrm{t}}}\right)$. Here Δn is negligible when compared with the difference of their group velocities Δn_{g}. By ignoring the effects of group velocity dispersion and higher order dispersion terms in CW cases, the overall THG phase mismatch can be given by

$$\Delta\beta_{\mathrm{total}}\approx\Delta\beta+\Delta\beta_{\mathrm{T}}+\Delta\beta_{\mathrm{Kerr}}=\frac{\Delta n_{\mathrm{g}}}{c}\left[\Omega_{\mathrm{t}}+\Omega_{\mathrm{TL}}(\delta T)+\Omega_{\mathrm{TNL}}(\Delta T)+\Omega_{\mathrm{KNL}}(I_{\mathrm{p}})\right]$$

$$\frac{\Delta n_{\mathrm{g}}}{c}\left[\Omega_{\mathrm{t}}+\xi_{\mathrm{t}}\omega_{\mathrm{t}0}\delta T+(\Theta_t+\mathrm{g}_{\mathrm{tp}})I_{\mathrm{p}}\right], \tag{S4.4}$$

where, $\Omega_{\mathrm{TL}} = \xi_{\mathrm{t}}\omega_{\mathrm{t}0}\delta T$ is linear TO phase mismatch determined by the chip temperature δT and $\Omega_{\mathrm{TNL}} = \Theta_{\mathrm{t}}I_{\mathrm{p}}$ is the nonlinear TO phase mismatch caused by the intra-cavity pump energy I_{p}. The overall nonlinear phase mismatch becomes $\Omega_{\mathrm{NL}} = \Omega_{\mathrm{TNL}} + \Omega_{\mathrm{KNL}} = (\Theta_{\mathrm{t}} + g_{\mathrm{tp}})\, I_{\mathrm{p}}$.

Section 5: Deterministic generation of athermal modes via THG

From Eq. (S4.4), when $\Delta\beta_{\text{total}} \approx 0$, we have

$$\Omega_{\text{t}} \approx -\xi_{\text{t}}\omega_{\text{t0}}\delta T - \left(\Theta_{\text{t}} + \text{g}_{\text{tp}}\right)I_{\text{p}} . \tag{S5.1}$$

The existence of athermal modes can be appreciated by calculating $\partial\Omega_{\text{t}}/\partial\text{T}$ from Eq. (S5.1), and setting it to zero, we have

$$I_{\text{p}}(\delta T) = -\frac{\xi_{\text{t}}\omega_{\text{t0}}}{\Theta_{\text{t}}+\text{g}_{\text{tp}}}\delta T = -\tau_{\text{t}}\delta T . \tag{S5.2}$$

Since $\delta T = T - T_0$, the cold cavity temperature T_0 was determined by $I_{\text{p}}(\delta T) = 0$ when $\delta T = 0$.

By bringing Eq. (S5.2) into Eq. (S3.2), we yield

$$\left[-i\Omega_{\text{p}} - i\xi_{\text{p}}\omega_{\text{p0}}\delta T - \frac{\kappa_{\text{p}}}{2}\right]a_{\text{p}} + i\Theta_{\text{p}}\tau_{\text{t}}\delta T a_{\text{p}} - i\sqrt{\kappa_{\text{pe}}}p_i = 0 , \tag{S5.3}$$

where, $\tau_{\text{p}} \approx \xi_{\text{p}}\omega_{\text{p0}}/\Theta_{\text{p}}$ is the compensation rate for the pump modes. If we define $\alpha = \frac{2\Omega_{\text{p}}}{\kappa_{\text{p}}}$, $\rho = -\frac{2\Theta_{\text{p}}\Delta\tau}{\kappa_{\text{p}}}\delta T = \frac{2\Theta_{\text{p}}\Delta\tau}{\kappa_{\text{p}}\tau_{\text{t}}}I_{\text{p}}$, and $F^2 = \frac{\Theta_{\text{p}}\Delta\tau}{\tau_{\text{b}}}\frac{8\kappa_{pe}}{\kappa_p^3}P_i$, as the normalized pump detuning, the normalized intra-cavity pump power, and the normalized intra-cavity pump power, respectively. Eq. (S5.3) can be written in the normalized form of

$$F^2 = [1 + (\rho - \alpha)^2]\rho . \tag{S5.4}$$

As discussed in ref.[S7], the athermal mode exists when $|\alpha| \geq \sqrt{3}$, which gives the critical values of normalized intra-cavity pump energy and input pump as

$$\rho_{\pm}(\alpha) = \frac{2\alpha \mp \sqrt{\alpha^2-3}}{3} , \tag{S5.5}$$

$$F_{\pm}^2(\alpha) = \frac{2\alpha \mp \sqrt{\alpha^2-3}}{3}\left[1 + \left(\frac{\alpha \pm \sqrt{\alpha^2-3}}{3}\right)^2\right] . \tag{S5.6}$$

From Eq. (S5.5), only when α is slightly larger than $\sqrt{3}$, the temperature range of the athermal mode can be maximized which looks like

$$|\delta T_+ - \delta T_-| = \rho_+ - \rho_- = \kappa_{\text{p}}\sqrt{\alpha^2 - 3}/(3\Theta_p\Delta\tau) . \tag{S5.7}$$

Moreover, from the condition $F^2 > \rho$ we can further characterize the temperature range of the athermal mode, which gives

$$P_i > \frac{\tau_{\text{t}}\kappa_{\text{p}}^2}{4\kappa_{\text{pe}}}|\delta T| = \frac{\pi R\omega_{\text{p}}^2 n_{0\text{p}}^2}{2v_{\text{ga}}}\frac{\tau_{\text{t}}}{\kappa_1^2 Q_{\text{p}}^2}|\delta T| , \tag{S5.8}$$

which indicates in the specific pump mode of MRR, the upper limit of δT is determined by the input pump power.

From Eq. (S5.4), when $F^2 > \rho$, we have

$$\alpha = \rho \pm \sqrt{\frac{F^2}{\rho} - 1} . \tag{S5.9}$$

Note that, since ρ has to be larger than zero, the smaller root of α cannot lead to an athermal mode. Therefore, Eq. (S5.9) gives the frequency detuning of the athermal pump mode as

$$\Omega_{\text{p}} = \Theta_{\text{p}}\Delta\tau|\delta T| + \sqrt{\frac{\kappa_{\text{pe}}P_i}{\tau_{\text{t}}|\delta T|} - \frac{\kappa_{\text{p}}^2}{4}} . \tag{S5.10}$$

The form of Eq. (S5.10) is similar to that of Eq. (S3.3). Both Eq. (S5.7) and Eq. (S5.10) indicate that $\Delta\tau$ with a slightly larger than zero value can provide a proper linear compensation rate to nonlinear TO phase mismatch across tens of degree temperature range for athermal operation.

Section 6: Determination of linear and nonlinear TO coefficients ratios τ_p

Figure S2(a) shows the measured cold-cavity resonance wavelengths of TE pump (blue squares) and TM pump (red circles) modes on corresponding chip temperature T in the C- and L-bands. With the core and claddings of the waveguide having different thermal coefficients, the TDWS of the pump modes are not identical and the resulting shift rate depends on the mode confinement of the specific modes. The measured linear TO coefficient ξ_p and the corresponding TDWS $d_p = \xi_p\lambda_p$ are shown in Table S2. It shows that, ξ_p of the TM mode increases and ξ_p of TE mode slightly reduces across the C- and L-bands. The measured TDWS is around 20 pm/°C for both the polarization modes, which is similar to the published values of ~21.1 pm/°C in SiN MRRs[S10] and 16 pm/°C in AlN/Si_3N_4 MRRs[S11] but much lower than in silicon waveguides[S12]. Figure S2b shows the transmission spectra at the drop port for the TE and TM modes when swept with a CW pump laser. The triangular response shapes are due to the intra-cavity power induced nonlinear TO resonance redshift[S10, S13–S14], which can effectively enhance the TH measurement window to 0.8 nm in highly doped silica glass MRRs, as shown in Fig. S2(b).

Moreover, it is important to note that the intra-cavity pump power can be determined directly from the detected drop power. Using the drop responses in Fig. S2b at the same input CW pump power, we calculated the nonlinear TO redshift rate Θ_p as shown in Table S2. For both TM and TE modes, Θ_p decreases when the resonance wavelength increases which is consistent with the results in ref.[S8]. We also noticed that the Θ_p of TE modes is larger than that of TM modes. Table S2 also shows the calculated τ_p. For TM modes, τ_p is doubled from C-band to L-band. Meanwhile, τ_p of TE modes are nearly the same in the bandwidth. Note that, Θ_p is two order of magnitudes larger than the Kerr nonlinear factor $g_{pp} = 7.16\times10^6\,\mathrm{pJ^{-1}}$ which corresponds to the measured Kerr nonlinear coefficient of the pump wave $\gamma_{pp} = 0.310\ \mathrm{W^{-1}\cdot m^{-1}}$ @ 1550 nm. It shows that for highly doped silica glass MRRs, the nonlinear TO effect is much stronger than the Kerr effect. For comparison, the ratio of Θ_p/g_{pp} is around 10 in silicon nitride waveguide[S15]. Therefore, it is reasonable to neglect Kerr nonlinearity induced phase mismatch in this work.

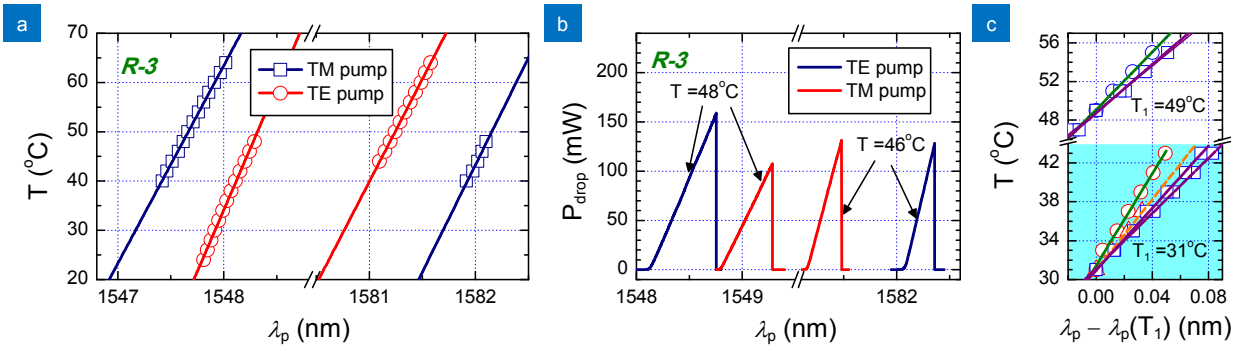

Fig. S2 | Determine the linear and nonlinear TO coefficients of the pump and TH modes. (**a**) Measured cold-cavity resonance locations vs chip temperature T. (**b**) Measured drop response of MRR (R-3). (**c**) TDWS rates comparison of three types of TH modes corresponding to Fig. 3(a). Since the TDWS rates have slightly difference in different temperature ranges, the TDWS rates are compared within 47°C ~ 55°C (upper) and 31°C ~ 45°C (lower).

Table S2 | The corresponding parameters of Fig. S2(a).

No.	Pump type	λ_{p0} (nm) @P_d = 1 mW	d_p (pm/°C)	ξ_p (1/°C)	Θ_p (rad/pJ)	τ_p (pJ/°C)	κ_1
1	TE	1547.62@48 °C	24.90	1.61×10^{-5}	1.87×10^{9}@48 °C	6.57	0.0691
2	TM	1548.29@48 °C	20.01	1.29×10^{-5}	1.68×10^{9}@48 °C	5.86	0.0610
3	TM	1581.15@46 °C	24.01	1.52×10^{-5}	0.94×10^{9}@46 °C	12.03	0.0670
4	TE	1582.06@46 °C	23.00	1.45×10^{-5}	1.41×10^{9}@48 °C	7.70	0.0775

References

[S1] Carmon, L. Yang, T. Vahala, K. J. Dynamical thermal behavior and thermal self-stability of microcavities. *Opt Express* **12**, 4742-4750 (2004).

[S2] Herr, T., Hartinger, K., Riemensberger, J., Wang, C. Y., Gavartin, E., Holzwarth, R. et al. Universal formation dynamics and noise of Kerr-frequency combs in microresonators. *Nature Photonics*, **6**, 480 (2012).

[S3] Guo, H. Karpov, M. Lucas, E. Kordts, A. Pfeiffer, M. H. P. Brasch, V. Lihachev, G. Lobanov, V. E. Gorodetsky, M. L. & Kippenberg, T. J. Universal dynamics and deterministic switching of dissipative Kerr solitons in optical microresonators. *Nat. Phys.* **13**, 94-102, (2017).

[S4] Rodriguez, A. Soljăcić, M. Joannopoulos, J. D. & Johnson, S. G. $\chi^{(2)}$ and $\chi^{(3)}$ harmonic generation at a critical power in inhomogeneous doubly resonant cavities. *Opt. Express* **15**, 7303-7318, (2007).

[S5] Liu, B. Yu, H. Li, Z. Y. & Tong, L. Phase-matched second-harmonic generation in coupled nonlinear optical waveguides. *J. Opt. Soc. Am. B.* **36**, 2650-2658 (2019).

[S6] Chembo, Y. K. & Menyuk, C. R. Spatiotemporal Lugiato-Lefever formalism for Kerr-comb generation in whisper cavity-gallery-mode resonators. *Phys. Rev. A* **87**, 053852 (2013).

[S7] Godey, C. Balakireva, I. V. Coillet, A. & Chembo, Y. K. Stability analysis of the spatiotemporal Lugiato-Lefever model for Kerr optical frequency combs in the anomalous and normal dispersion regimes. *Phys. Rev. A* **89**, 063814 (2014).

[S8] Li, Y. Wang, S. H. Tian, Y. Ho, W. L. Li, Y. Wang, L. Davidson, R. R. Little, B. E. & Chu, S. T. Third-harmonic generation in CMOS-compatible highly doped silica micro-ring resonator. *(accepted to be published in Optics Express).*

[S9] Agrawal, G. P. Nonlinear fiber optics 4th edn, (Elsevier, 2009).

[S10] Xue, X. Xuan, Y. Wang, C. Wang, P. H. Liu, Y. Niu, B. Leaird, D. E. Qi, M. & Weiner, A. M. Thermal tuning of Kerr frequency combs in silicon nitride microring resonators. *Opt. Express* **24**, 687-698, (2016).

[S11] Surya, J. B. Guo, X. Zou, C. L. & Tang, H. X. Efficient third-harmonic generation in composite aluminum nitride/silicon nitride microrings. *Optica* **5**, 103-108, (2018).

[S12] Guha, B. Cardenas, J. Lipson, M. Athermal silicon microring resonators with titanium oxide cladding. Opt. Express 21, 26557–26563 (2013).

[S13] Ikeda, K. Saperstein, R. E. Alic, N. & Fainman, Y. Thermal and Kerr nonlinear properties of plasma-deposited silicon nitride/ silicon dioxide waveguides. *Opt. Express* **16**, 12987–12994 (2008).

[S14] Lee, J. M. in Silicon Photonics III: Systems and Applications 1st edn, (eds Pavesi, L. & Lockwood D. J.) Ch. 3 (Springer, 2016).

[S15] Bao, C. Xuan, Y. Jaramillo-Villegas, J. A. Leaird, D. E. Qi, M. & Weiner, A. M. Direct soliton generation in microresonators. *Opt. Lett.* **24**, 2519-2522, (2017).